BIOCHEMISTRY
including biophysical chemistry & molecular biology

Article

pubs.acs.org/biochemistry

DNA Binding Regulates the Self-Association of the ETS Domain of PU.1 in a Sequence-Dependent Manner

Gregory M. K. Poon*

Department of Pharmaceutical Sciences, Washington State University, Pullman, Washington 99164-6534, United States

Supporting Information

ABSTRACT: The current paradigm of ETS transcription factors holds that their DNA-binding (ETS) domain binds to a single sequence-specific site with strict 1:1 stoichiometry. PU.1 (Spi-1) is a lineage-restricted member of the ETS family that is essential in normal hematopoietic development. Characterization of the binding properties of the ETS domain of PU.1 by isothermal titration calorimetry revealed that it binds a single sequence-specific binding site with 1:1 and 2:1 stoichiometry in a discrete, sequential, and negatively cooperative manner. While both high-affinity- and low-affinity-specific sites exhibit this behavior, the thermodynamics for each complex are highly differentiated. In the unbound state, the PU.1 ETS domain exists as a weak noncovalent homodimer that dissociates and unfolds cooperatively. Thus, the PU.1 ETS domain exists as a monomeric and dimeric species in both DNA-bound and free states. Structural characterization of the protein−DNA interface by quantitative DNA footprinting revealed new minor groove contacts and changes in the core consensus suggestive of increased DNA distortion in the 2:1 complex. Together, the structural and thermodynamic data support a model in which DNA binding dissociates a PU.1 ETS dimer to a 1:1 protein−DNA complex followed by, at higher concentrations, an asymmetric 2:1 complex. The implications of distinct monomeric and dimeric states on the known structural biology of ETS domains as well as potential ETS−protein interactions are discussed.

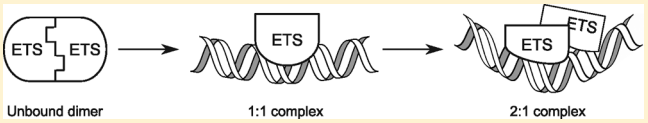

ETS proteins comprise a functionally diverse family of transcription factors distributed throughout the Metazoa. All ETS proteins share a structurally conserved, eponymous DNA-binding domain that recognizes a large repertoire of sites harboring a central 5′-GGAA-3′ consensus.[1,2] This core consensus is contacted by an essential recognition helix in the ETS domain that belongs to the winged helix−turn−helix family.[3] Although combinatorial control is a major principle in the biology of ETS proteins, the intrinsic sequence selectivity of the ETS domain plays an at least equally important role in gene transactivation. This is evidenced by the exact correspondence between binding affinity and transactivational activity,[4] as well as the prevalence of high-affinity sequences identified in vitro among ETS binding sites in vivo.[1,2] There are at least two mechanisms by which these two features are accommodated. One mechanism is illustrated by the recruitment of IRF-4 by the ETS domain of PU.1 (Spi-1) at the λB motif of the Igλ$_{2-4}$ enhancer. In the PU.1−/IRF-4−DNA ternary complex,[5] the λB motif harbors overlapping high-affinity binding sequences for the two proteins, thereby facilitating their colocalization on the DNA.

A second mechanism by which combinatorial control and intrinsic sequence selectivity play complementary roles is that in which the ETS domain mediates interactions in addition to DNA recognition. Although the ETS domain is primarily known as a DNA-binding domain, protein−protein interactions with other domains and binding partners are increasingly coming to light. The allosteric regulation of DNA binding by autoinhibitory domains in Ets-1 represents the best-studied example.[6] A variety of protein−protein contacts involving the ETS domain have been observed in DNA-bound ternary structures, including GABPα/β,[7] SAP-1/SRF,[8] Ets-1/Pax-5,[9] and Ets-1/CBFα2.[10,11] In the unbound state, the ETS domains of full-length PU.1, Ets-1, Elk-1, and ERG mediate the formation of homo- and heterotypic complexes.[12−14] These interactions are biologically relevant, as demonstrated in the case of Elk-1, by the effects of ETS-mediated homodimerization on cytoplasmic stability against proteosomal degradation and localization to the nucleus.[13] We are particularly intrigued by the report that in live cells PU.1 homodimerizes in the nucleus but appears to bind high-affinity sites only as monomers.[13] Because the ETS domain of PU.1 binds a large number (>70) of cognate DNA sites with a dispersion of affinities,[2,15] the question of whether sequence selectivity may be manifest in terms of preferential protein−protein interactions arises. We have conducted a detailed biophysical characterization of the DNA binding properties of the PU.1 ETS domain in solution. A combination of calorimetric, spectroscopic, biochemical, and footprinting techniques indicates that the ETS PU.1 domain exists as monomers and dimers in both free and DNA-bound states at equilibrium. Unusually, the PU.1 ETS domain is capable of forming a discrete 2:1 protein−DNA complex. To date, binding of ETS oligomers to a single DNA binding site has not been reported. Analyses of the thermodynamics of binding and the protein−DNA interface reveal new interactions in the 2:1 complex. The impact of the 2:1 complex on the known structural biology of ETS domains and the implications

Received: March 11, 2012
Revised: April 16, 2012
Published: April 26, 2012

   dx.doi.org/10.1021/bi300331v | *Biochemistry* 2012, 51, 4096−4107

of the interplay between DNA binding and self-association of the PU.1 ETS domain in the full-length protein are discussed.

EXPERIMENTAL PROCEDURES

Protein Preparation. The PU.1 ETS domain (residues 167−262 from the murine sequence) was cloned into the pQE-60 vector (Qiagen), overexpressed in *Escherichia coli* M15-[pREP4], and purified as previously described.[16] The final purified protein was free of a purification tag. The concentration was determined by UV spectrometry (ε_{280} = 22460 M^{-1} cm^{-1}).

Isothermal Titration Calorimetry. Complementary oligonucleotides (23 bp) harboring a single ETS binding site were mixed at equimolar ratios of ∼0.5 mM, heated in a boiling water bath for 5 min, and annealed by being cooled overnight to room temperature. DNA and purified PU.1 ETS domain (concentrated to ∼1 mM) were extensively codialyzed against the same buffer [50 mM NaH_2PO_4/Na_2HPO_4 (pH 7.4) and 150 mM total Na^+] in separate dialysis units (D-Tubes Mini, EMD Biochemicals). Dialysate from the final round was used in all subsequent dilution, blanking, and rinsing procedures. ITC was conducted using a NanoITC instrument (TA Instruments, Logan, UT). Both forward (protein into DNA) and reverse (DNA into protein) titrations were performed. Typically, 100 μL of titrant (∼400 μM) was titrated in 5 μL increments every 300 s into a cell volume of 975 μL (∼10 μM titrate or buffer) with stirring at 300 rpm. Exact concentrations were determined by UV spectrometry prior to each experiment. The extinction coefficient of dsDNA was calculated from nearest-neighbor parameters.[17] Thermograms were assigned baselines, and peaks were integrated numerically and converted into heat per mole of titrant. Model-free determination of calorimetric enthalpies (ΔH_{cal}) was conducted by computing recursive two-tailed prediction intervals (PI) for j consecutive measurements ($j > 3$) beginning with the first point after a nominal equivalence point:

$$\mathrm{PI}_j = \hat{q}_j \pm t_{1-\alpha/2k,j-1}\hat{s}_j\sqrt{1+\frac{1}{j}} \quad (1)$$

where $\hat{q}_j$ is the current estimate of the mean titration heat (per mole of titrant), $\hat{s}_j$ is the current estimate of the standard deviation, and $t_{1-\alpha/2k,j-1}$ is the Student's t statistic at α = 0.05 and $j-1$ degrees of freedom. If the next k = 2 measurements lie outside PI_j, the iteration is stopped and

$$\Delta H_{cal} = \hat{q}_j \pm \frac{\hat{s}_j}{\sqrt{j}} \quad (2)$$

Model-dependent parameter estimation was performed by nonlinear regression as described previously.[18]

Glutaraldehyde Cross-Linking. Samples were prepared in phosphate buffer as used in ITC experiments and treated with aqueous glutaraldehyde (Sigma-Aldrich) at 0.025% (w/v). At various time points, aliquots were quenched in standard SDS loading buffer, denatured at 90 °C for 3 min, and resolved by sodium dodecyl sulfate−polyacrylamide gel electrophoresis (SDS−PAGE). Gels were stained with Coomassie Blue G-250 and scanned with a LI-COR Odyssey Instrument at the 680 nm channel.

Size-Exclusion Chromatography. Samples were filtered at the 0.45 μm level and loaded onto a Superdex 30/200 column connected to an ÄKTA purifier instrument (GE Healthcare). The mobile phase was 10 mM NaH_2PO_4/Na_2HPO_4 (pH 7.4) flowing at a rate of 0.5 mL/min at ambient temperature. Analytes were detected by UV absorption at 280 nm. The column was calibrated using protein standards (Sigma-Aldrich).

Light Scattering Experiments. Static and dynamic scattering by the unbound PU.1 ETS domain was performed using a Zetasiser Nano ZS90 instrument (Malvern, Worcestershire, U.K.). Samples were irradiated with a 633 nm He−Ne source, and scattering was detected at 90°. Attenuation of source radiation and measurement position were controlled by software. The purified PU.1 ETS domain was concentrated to ∼1 mM and extensively dialyzed against phosphate-buffered saline. The concentration of the dialyzed protein was measured by UV spectrometry after it had been filtered at the 0.45 μm level. Each measurement was taken for 10 s following equilibration for 120 s. The molecular mass was determined from SLS data by extrapolation of a Debye plot, or DLS via the Mark−Houwink relation. The polydispersity was assessed in terms of the polydispersity index as prescribed by ISO13321 (1996). Technique and instrumental performance were verified using commercially purified bovine serum albumin (EMD) and lysozyme (Sigma-Aldrich).

Filter Binding Experiments. Experimental procedures were as previously described[15,19] with modifications.[16] van't Hoff analysis was performed as described previously.[20]

Quantitative DNA Footprinting. An ∼130 bp fragment harboring a single 23 bp ETS binding site was cloned into the *Eco*RI and *Hin*dIII sites of pUC19. The fragment was radiolabeled at a single 5′-end with [γ-^{32}P]ATP by polymerase chain reaction (PCR) and purified from an agarose gel as described previously.[16] ETS−DNA binding was performed in 50 μL of binding buffer [10 mM NaH_2PO_4/Na_2HPO_4 (pH 7.4) and 150 mM total Na^+] containing ∼1 nM singly labeled DNA fragment, PU.1 ETS domain as indicated, acetylated bovine serum albumin (100 ng/μL), and poly-d(AT)·poly-d(AT) (10^{-5} M bp). At equilibrium, enzymatic or chemical footprinting was performed under conditions that introduced <30% total cleavage to maximize the fraction of singly cleaved DNA. Selected chemical sequencing reactions were performed for base identification. DNase I, hydroxyl radical, and permanganate footprinting were performed as described previously.[21−23] Cleaved DNA was extracted with a phenol/chloroform/isoamyl alcohol mixture, washed with diethyl ether, and precipitated with ethanol. Purified DNA was separated by standard denaturing electrophoresis. Gels were digitized by phosphorimagery using a Storm 860 instrument (GE Healthcare), and lane traces were fit to a superposition of Lorenztian functions without a baseline.[24]

RESULTS

The ETS Domain of PU.1 Binds DNA at Multiple Stoichiometries. Isothermal titration calorimetry (ITC) was used to measure the binding of the ETS domain of PU.1 to double-stranded oligonucleotides harboring a single copy of a sequence-specific binding site (Figure 1). These sites are related to the λB motif of the Ig2-4 enhancer and were chosen to achieve a wide range of affinities (Table 1).[25] When the reactions were performed as "forward" titrations (protein into DNA), the data revealed significant titration heats beyond the 1:1 equivalence point for all sites examined. In every case, the signals returned to baseline after a second equivalence point at a 2:1 protein:DNA ratio. The two "equivalents" of titration heats are distinguishable in magnitude and, in the case of the [−]GC and [+]TG site, opposite in sign. Not unexpectedly, model fitting to a single class of sites required non-zero baselines and site

dx.doi.org/10.1021/bi300331v | *Biochemistry* 2012, 51, 4096−4107

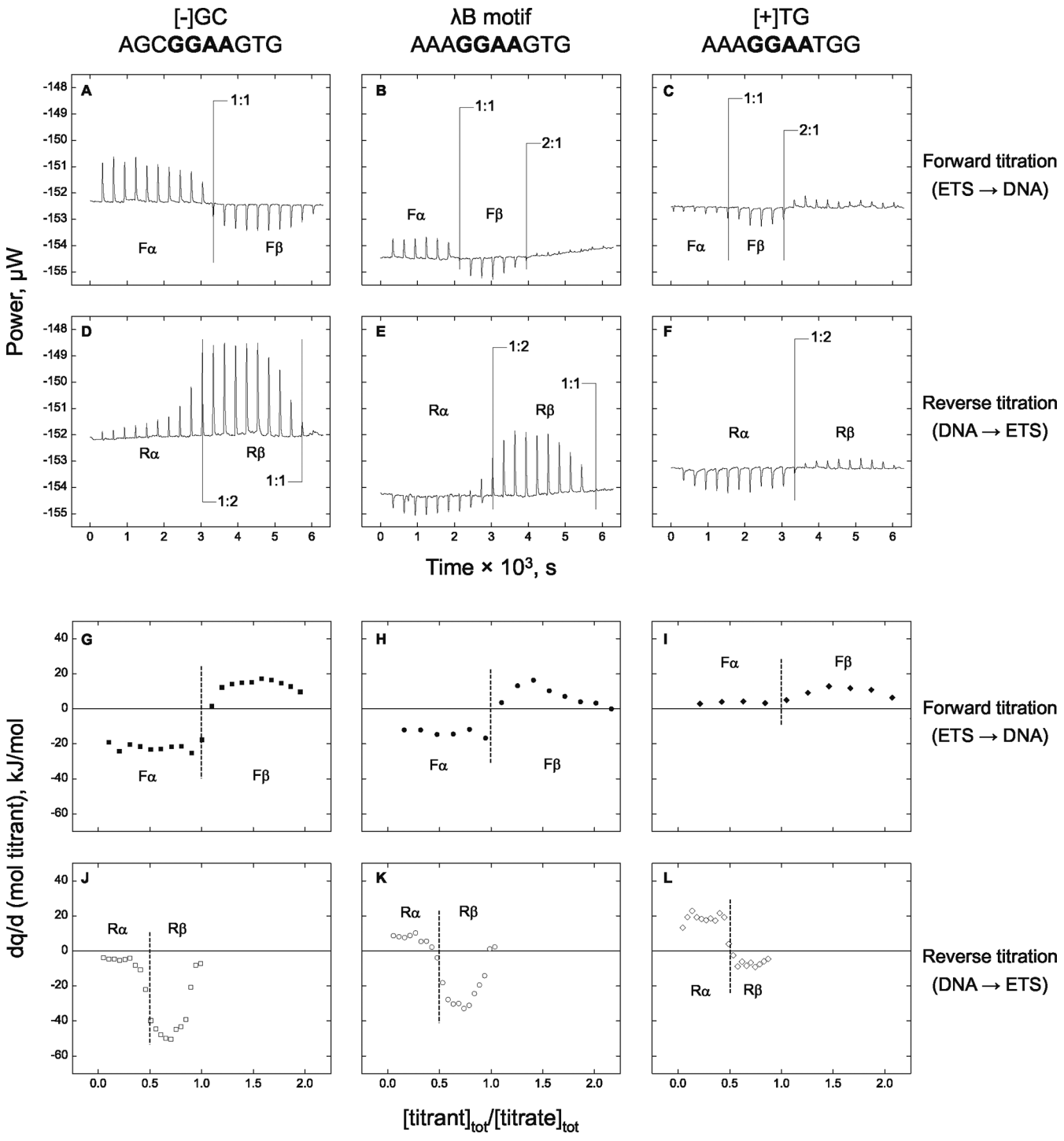

Figure 1. ETS domain of PU.1 that binds DNA at multiple stoichiometries. Sequence-specific binding by the PU.1 ETS domain was probed by isothermal titration calorimetry. Details of the three specific sites are given in Table 1. (A–F) Representative thermograms of forward [protein as titrant (A–C)] and reverse [DNA as titrant (D–F)] titrations recorded at 25 °C. Upward peaks represent exothermic reactions. The ratios are the nominal titrant:titrate equivalence points as determined from the total concentrations of titrant and titrate, which were measured independently by UV spectrometry before each experiment. The abscissa and ordinate for each panel are normalized to the same scale; the slight offset in the baselines is due to the use of different injection syringes in the experiments. Fα, Fβ, Rα, and Rβ represent titration heats bracketed by the indicated equivalence points. (G–L) Numerically integrated heats from the thermograms shown in panels A–F. The abscissa and ordinate are normalized to the same scale. Titrant concentrations are shown in terms of molar titrant:titrate ratios from 0 to 2.0; absolute titrate concentrations range from 10 to 50 μM (PU.1 ETS domain in the forward titrations; DNA duplexes in the reverse titrations). The 1:1 and 1:2 equivalence points in the forward (G–I) and reverse (J–L) titrations, respectively, are marked with dashed lines to aid visualization. Points beyond these equivalence points (dilution heats) in some titrations are off this scale.

parameters significantly above unity (Figure S1 of the Supporting Information). These observations can be reproduced with independent preparations of proteins and oligonucleotides. Similar biphasic results were observed with an alternate buffer [10 mM

dx.doi.org/10.1021/bi300331v | *Biochemistry* 2012, 51, 4096–4107

Table 1. Sequences of the Sequence-Specific PU.1 ETS Binding Sites Studied[a]

Site[b]		[-] flanking segment	Core	[+] flanking segment		Relative affinity[c]
[-]GC		AGC TCG	**GGAA** **CCTT**	GTG CAC		1
λB	GCGAATA CGCTTAT	AAA TTT	**GGAA** **CCTT**	GTG CAC	AAACCG TTTGGC	0.2
[+]TG		AAA TTT	**GGAA** **CCTT**	TGG ACC		2×10^{-3}

[a]These sequences were used as shown in synthetic oligonucleotides in ITC and filter binding experiments. Terminal GCG trinucleotides were added to minimize fraying at the ends. For footprinting experiments, each sequence was embedded in a PCR-amplified fragment (~130 bp) as described in Experimental Procedures. [b]The notations [−] and [+] refer to positions 5′ and 3′, respectively, from the core in the GGAA strand; the letters refer to base substitutions relative to the native λB motif. [c]Relative affinities were calculated from data reported by Poon and Macgregor.[15]

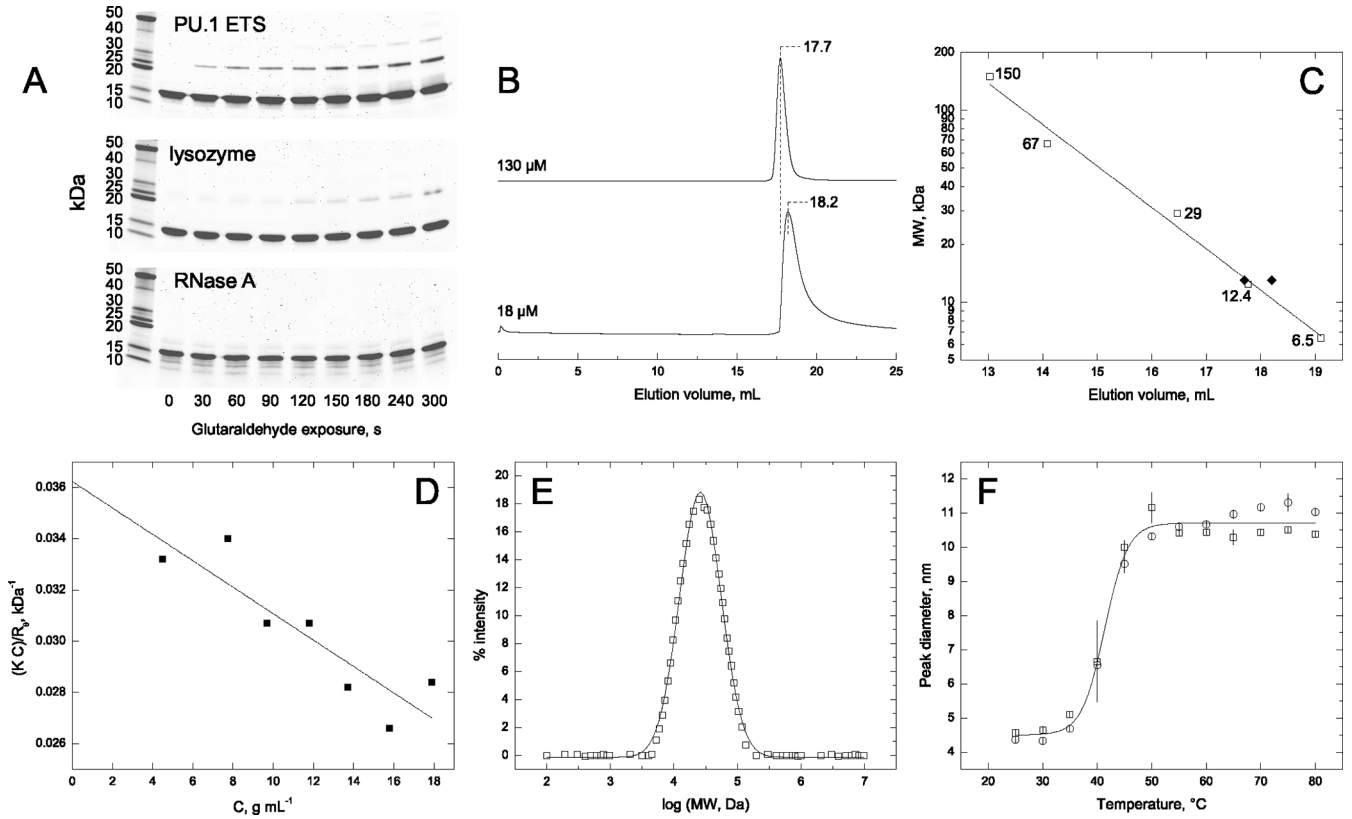

Figure 2. Unbound ETS domain of PU.1 that self-associates in solution. (A) The PU.1 ETS domain, chicken egg white lysozyme, or RNase A (250 μM) was identically treated with glutaraldehyde and resolved by SDS−PAGE. Each sample lane represents 1.0 μg of total sample. Molecular mass markers are as indicated. (B) SEC profiles for the PU.1 ETS domain at two different loading concentrations, scaled to the same peak height. (C) Molecular mass estimation by SEC. The column was calibrated with globular protein standards as labeled. The interpolated apparent molecular masses for the two samples shown in panel B are 13.4 and 10.4 kDa for the 130 and 18 μM samples (◆), respectively. (D) Representative Debye plot of SLS measurements. *C* denotes the protein concentration in grams per milliliter. κ is an optical constant. R_θ is the Rayleigh ratio. The instrumental imprecision at this level of signal is approximately 10−15%. The extrapolated intercept at the ordinate represents the reciprocal apparent molecular mass in kilodaltons. (E) Representative MW distribution as measured by DLS. Hydrodynamic size data were converted to apparent molecular mass via the Mark−Houwink relation assuming spherical geometry. Averaged data from all LS experiments are listed in Table 2. (F) DLS-detected thermal denaturation of the PU.1 ETS domain at 0.9 mM monomer. The symbols represent data from two independent experiments, each of which is an average (±SE) of duplicate measurements at each temperature step. The curve represents an empirical fit to a sigmoidal function to aid visualization.

sodium cacodylate (pH 6.8)]. SDS−PAGE and size-exclusion chromatography revealed no detectable heterogeneity in the purified protein (Figure 2A,B). Finally, we performed extensive control experiments (e.g., buffer−buffer titrations and different injection syringes) to ensure that the observations were not an artifact of our technique.

If the apparent stoichiometries are intrinsic to the system, they should also be manifest in reverse titrations (DNA into protein). Indeed, two distinct equivalents of titration heats were observed with equivalence points at protein:DNA ratios of 1:2 and 1:1. The magnitudes and signs of the titration heats are different from those observed in the forward titrations. Thus,

dx.doi.org/10.1021/bi300331v | *Biochemistry* 2012, 51, 4096−4107

multiple states of DNA binding are intrinsic to the PU.1 ETS domain. Moreover, the clear separation of the two phases in the forward (Fα and Fβ) and reverse (Rα and Rβ) titrations implies that the two binding events are negatively cooperative with respect to each other.

Taken in isolation, the reverse titration data suggest negatively cooperative binding by a dimeric protein (Figure S1 of the Supporting Information). However, the forward titrations reveal no negative cooperativity (or any other detectable heterogeneity) between the two presumptive sites in the Fα phase. In addition, the 2:1 stoichiometry observed in the forward titrations is incompatible with such a scheme. We therefore propose Scheme 1 to account for the equilibrium

Scheme 1

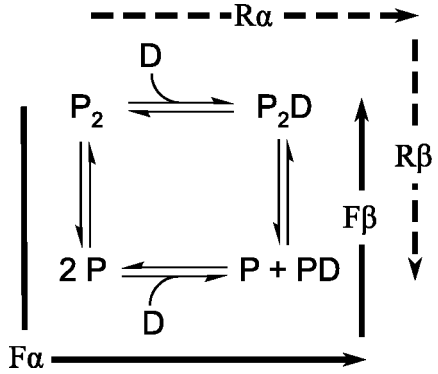

binding properties in both titrations: P and D represent the PU.1 ETS domain and a specific DNA binding site, respectively. Fα, Fβ, Rα, and Rβ represent the four observed phases of titration heats (Figures 1A–F). Thus, Scheme 1 proposes four possible states for the PU.1 ETS domain at equilibrium: namely, monomers and dimers in both DNA-bound and free states. In the following sections, we report independent experiments aimed at assessing the validity of Scheme 1.

The PU.1 ETS Domain Is a Noncovalent Dimer in Solution. Because Scheme 1 requires a dimeric PU.1 ETS domain in the unbound state, we set out to determine the unbound protein's stoichiometry. Cross-linking experiments using glutaraldehyde (Figure 2A), followed by denaturing electrophoresis, revealed a new species at twice the formula mass of the PU.1 ETS monomer (13.0 kDa). To distinguish between a true equilibrium dimer and potential trapped products of nonspecific, transient collisions, we cross-linked two other proteins of similar molecular mass at identical concentrations (250 μM). Chicken egg white lysozyme dimerizes weakly under physiologic conditions ($K \sim 10^2$),[26,27] while RNase A is not known to oligomerize. Comparison of the three electrophoretic patterns clearly suggests a specific equilibrium dimer for the PU.1 ETS domain. Under native conditions, size-exclusion chromatography showed increasing peak lag and tailing with a decreasing input concentration, indicative of a noncovalent oligomer in exchange with dissociated subunits (Figure 2B). Because elution volumes are reproducible to ±0.05 mL, the differences in the line shapes should be considered significant. Although the protein eluted at volumes close to that of the monomer (Figure 2C), this is likely due to excess adsorption of the protein (pI = 10.6) to negative charges (carboxylates, ~1 μmol/mL) on the Superdex 200 medium.[28] We therefore turned to light scattering for a solution state characterization. At concentrations from 0.2 to 0.9 mM, both static and dynamic light scattering measurements gave an apparent molecular mass that was twice the formula mass (Table 2). Neither probe revealed significant polydispersity at

Table 2. Molecularity of the Unbound ETS Domain of PU.1[a]

probe	apparent molecular mass (kDa)	molecularity[d]
SLS[b] (N = 8)	28.9 ± 2.9	2.2 ± 0.2
DLS[c] (N = 9)	24.9 ± 1.3	1.9 ± 0.1

[a]Static and dynamic light scattering measurements are reported as means (±SE) of N replicate experiments as indicated. Representative replicates are shown in panels D and E of Figure 2. [b]Measurements at monomer concentrations from 0.2 to 0.9 mM. [c]Measurements at 0.9 mM monomer. The mean hydrodynamic diameter was 4.4 ± 0.1 nm. The mean polydispersity index was 0.11 ± 0.1. [d]Molecularity was computed on the basis of a formula mass of 13.0 kDa for the PU.1 ETS domain.

the protein concentrations used. DLS-detected thermal melting (at 0.9 mM protein) showed a monophasic, sigmoidal increase in particle size from 4.5 ± 0.1 to 10.7 ± 0.1 nm with an apparent melting temperature of 41.4 ± 0.3 °C (Figure 2F). This value is significantly lower than that in experiments using lower concentrations of the PU.1 ETS domain as detected by circular dichroism and differential scanning calorimetry (~50 °C at up to 40 μM).[29,30] The lack of an intermediate state corresponding to a folded monomer in the DLS melts suggests that dimer dissociation and unfolding are coupled at equilibrium. This is consistent with an apparent loss of binding and large dilution heats in ITC forward titrations (protein concentrations of 10^{-4} M in the syringe) conducted at 45 °C (data not shown), in contrast with noncalorimetric titrations (protein concentrations of $\leq 10^{-5}$ M) that routinely tolerate such temperatures (cf. Figure 3).

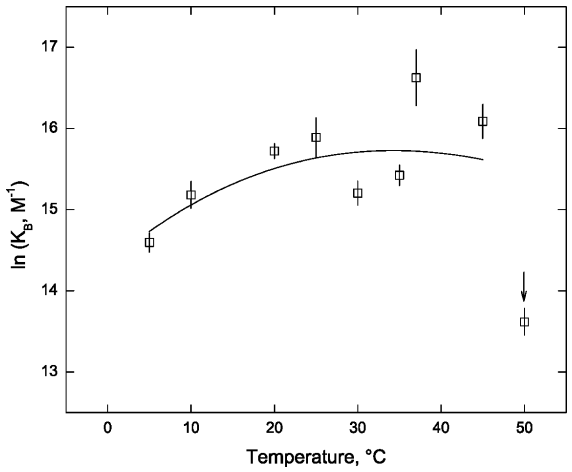

Figure 3. Thermodynamics of low-affinity sequence-specific binding by the PU.1 ETS domain. Binding to the low-affinity [+]TG site was measured at equilibrium by filter binding at the indicated temperatures. Values on the ordinate represent fitted estimates of binding affinities (±SE) and converted to ln K_B = ln(1/K_D). The curve represents an error-weighted fit of the data to the van't Hoff equation assuming a temperature-independent change in heat capacity.[20] The 50 °C point (marked by an arrow) was excluded from the fit. Note that the binding constant is increasing through 25 °C, indicating a positive $\Delta H°$ at that temperature.

Table 3. Calorimetric Enthalpies of Forward and Reverse Titrations of PU.1 ETS Domain−DNA Interactions at 25 °C

		ΔH_{cal}[a] (kJ/mol)				
site	[Na^+] (mM)	Fα	Fβ	Fα + Fβ[b]	Rα	Rβ
[−]GC	150	−29.7 ± 0.3	15.6 ± 0.7	−5.0 ± 0.9	−4.8 ± 0.2	−45.7 ± 1.4
	250	−22.9 ± 0.1	8.3 ± 1.1	−13.1 ± 1.1	−13.7 ± 2.7	−25.1 ± 2.2
λB	150	−10.3 ± 0.1	15.5 ± 0.9	6.7 ± 0.9	8.6 ± 0.3	−29.9 ± 1.4
[+]TG	150	3.9 ± 0.3	10.2 ± 1.3	15.6 ± 1.3	14.9 ± 1.2	−8.4 ± 1.1
	250	8.3 ± 0.2	10.9 ± 1.8	20.7 ± 0.5	21.1 ± 2.8	−0.5 ± 0.8

[a]Calorimetric enthalpies were extracted from observed heats of titration according to eq 2 as described in Experimental Procedures. Each value includes a small contribution from the injection heat (−1.5 ± 0.2 kJ/mol titrant from dilution experiments) and is the mean (±SE) of up to three independent experiments. Fα, Fβ, Rα, and Rβ are as labeled in Figure 1 and described in the text. [b]The summed enthalpies of the two phases in the forward titration, corresponding to $\Delta H_{R\alpha}$ according to Scheme 1 (eq 5). One equivalent of injection heat was subtracted for comparison with $\Delta H_{R\alpha}$.

In summary, the aggregate results of biochemical and biophysical characterization of the unbound PU.1 ETS domain are consistent with a reversible dimer dissociating in the 10^{-5}–10^{-4} M range.

Thermodynamic Analysis of PU.1 ETS Domain−DNA Interactions. Scheme 1 constitutes a thermodynamic cycle. As such, conservation of thermodynamic properties offers a test for self-consistency, as well as insight into the molecular processes involved. Following Scheme 1, the apparent enthalpy changes for the two phases observed in the forward titrations ($\Delta H_{F\alpha}$ and $\Delta H_{F\beta}$) and the two phases for the reverse titrations ($\Delta H_{R\alpha}$ and $\Delta H_{R\beta}$) may be interpreted as follows:

$$\Delta H_{F\alpha} = \Delta H_{P_2 \rightarrow 2P} + \Delta H_{P+D \rightarrow PD} \quad (3)$$

$$\Delta H_{F\beta} = \Delta H_{P+PD \rightarrow P_2D} \quad (4)$$

$$\Delta H_{R\alpha} = \Delta H_{P_2+D \rightarrow P_2D} = \Delta H_{F\alpha} + \Delta H_{F\beta} \quad (5)$$

$$\Delta H_{R\beta} = -\Delta H_{P+PD \rightarrow P_2D} + \Delta H_{P+D \rightarrow PD} \quad (6)$$

According to eq 5, the summed enthalpy changes for the two phases of the forward titration (Fα and Fβ) correspond to that of the first phase of the reverse titration (Rα). We computed calorimetric (model-free) enthalpies for the forward and reverse titrations (Table 3) and found good agreement with eq 5. We repeated the forward and reverse titrations for the [−]GC and [+]TG sites at 250 mM Na^+ and again found agreement with eq 5. Because the forward and reverse titrations, as well as the two Na^+ concentrations studied, represent independent experiments, random agreement with eq 5 is highly improbable. We conclude therefore that Scheme 1 correctly describes the binding properties of the PU.1 ETS domain.

With a viable model in hand, we proceed to manipulate eqs 3−6 to reveal thermodynamic properties of the various states of the PU.1 ETS domain (Table 4). The enthalpy change for the formation of the 1:1 complex is not directly given by any of the four observed calorimetric enthalpies but can be inferred from the following:

$$\Delta H_{R\beta} + \Delta H_{F\beta} = \Delta H_{P+D \rightarrow PD} \quad (7)$$

At both 150 and 250 mM Na^+, high-affinity binding (to the [−]GC and λB sites) is strongly enthalpy-driven, in agreement with published van't Hoff enthalpies for high-affinity binding sites (dissociation constants of $<10^{-7}$ M).[19] A positive enthalpy change for the [+]TG site is inferred at 25 °C, suggesting that a low-affinity but sequence-specific complex can be entropy-driven. As another independent test of Scheme 1, we measured the temperature dependence of the equilibrium constant for the [+]TG site by filter binding under similar solution conditions (Figure 3). The equilibrium binding constant is very weakly dependent on temperature from 4 to 45 °C but is clearly increasing at 25 °C, corresponding to a positive enthalpy change. $\Delta H°$ reaches zero at ∼34 °C. The associated change in heat capacity (ΔC_p) is negative in sign (approximately −1.6 kJ mol^{-1} K^{-1}) and less than half the magnitude reported for both high-affinity sites.[19] Its magnitude is within experimental uncertainty.

Table 4. Enthalpy Changes for the Formation of Homotypic and DNA Complexes of the PU.1 ETS Domain at 25 °C[a]

site	[Na^+] (mM)	1:1 complex[b]	1:2 complex[c]	DNA-free dimer[d,e]
[−]GC	150	−27.1 ± 1.6	17.1 ± 0.7	1.1 ± 1.6
	250	−13.8 ± 2.5	9.8 ± 1.1	7.6 ± 2.5
λB	150	−11.4 ± 1.7	17.0 ± 0.9	−2.6 ± 1.7
[+]TG	150	4.8 ± 1.7	11.7 ± 1.3	−0.6 ± 1.8
	250	13.4 ± 2.0	12.4 ± 1.8	3.7 ± 1.0

[a]Enthalpy changes (in kilojoules per mole) were derived from calorimetric enthalpies according to eqs 4, 7, and 8. A correction for the injection heat (−1.5 ± 0.2 kJ/mol titrant from dilution experiments) was applied in each case. The uncertainties shown were calculated by standard procedures of error propagation. [b]From eq 7: $\Delta H_{R\beta} + \Delta H_{F\beta}$. [c]Addition of the second equivalent of protein to the 1:1 complex, i.e., $\Delta H_{F\beta}$ (eq 4). [d]From eq 8: $\Delta H_{R\beta} + \Delta H_{F\beta} - \Delta H_{F\alpha}$. [e]Mean value and standard deviation calculated from data for the three sites (−0.7 ± 1.8 kJ/mol at 150 mM Na^+). At 250 mM Na^+, the value from the [−]GC site should be considered more accurate because $\Delta H_{R\beta}$ is near zero for the [+]TG site.

The change in enthalpy for the formation of the 2:1 complex from the 1:1 complex is directly provided by $\Delta H_{F\beta}$ (eq 4). The thermodynamics are also sequence-dependent (Table 4) but altogether different from those of the 1:1 complex. Specifically, the 2:1 complex is strongly entropy-driven for all sites throughout the experimental temperature range (Figure 4). Unlike the order observed for the 1:1 complex,[19] $\Delta C_{p,\beta}$ for the high-affinity [−]GC site is less negative (smaller in magnitude) than for the low-affinity [+]TG site, with the enthalpy changes crossing over at ∼20 °C in 150 mM Na^+. In addition, $\Delta H_{F\beta}$ is salt-sensitive for the [−]GC site, but not the [+]TG site. Thus, the calorimetric data demonstrate that the physical driving forces that stabilize the 1:1 and 2:1 complexes are very different as well as sequence-dependent.

Finally, to obtain the enthalpy change for dimerization of the unbound PU.1 ETS dimer ($-\Delta H_{P_2 \rightarrow 2P}$), we note that

$$\Delta H_{R\beta} + \Delta H_{F\beta} - \Delta H_{F\alpha} = -\Delta H_{P_2 \rightarrow 2P} \quad (8)$$

dx.doi.org/10.1021/bi300331v | Biochemistry 2012, 51, 4096−4107

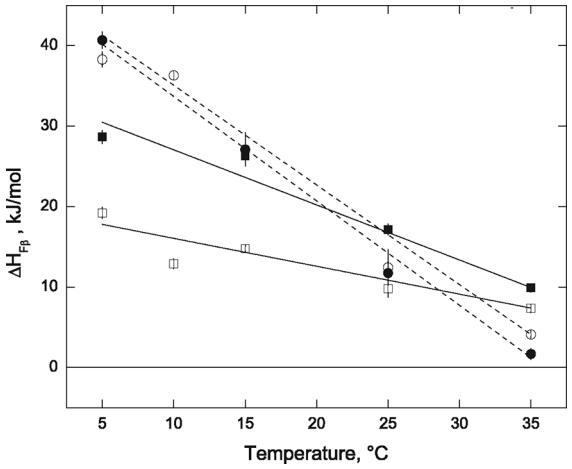

Figure 4. Thermodynamics of the 2:1 PU.1 ETS domain–DNA complex. Model-free calorimetric enthalpies for the Fβ phase were computed from forward titration heats as described in Experimental Procedures. $\Delta H_{F\beta}$ represents the enthalpy change for binding the second equivalent of the PU.1 ETS domain to form the 2:1 complex (eq 4). The temperature dependence of $\Delta H_{F\beta}$ (ΔC_p) for the high-affinity [−]GC (squares and solid lines) and low-affinity [+]TG (circles and dashed lines) sites at 150 mM Na^+ (filled symbols) and 250 mM Na^+ (empty symbols).

$\Delta H_{P_2 \rightarrow 2P}$ should depend on solution conditions but not the binding site considered. Application of eq 8 gave a mean value of ~0 (within experimental uncertainty) at 150 mM Na^+ for the three sites. Via characterization of the unbound PU.1 ETS domain, the small enthalpies are unlikely to be due to the absence of unbound dimers at the protein concentrations in the ITC experiments (>200 μM in the syringe). Rather, they reflect the entropic nature of the interactions stabilizing the unbound PU.1 ETS dimer.

Quantitative DNA Footprinting Titrations. The highly differentiated thermodynamics that underlie the sequential binding of PU.1 ETS domains to a single DNA site imply correspondingly differentiated structural transitions. To characterize the concentration-dependent structures of the PU.1 ETS domain–DNA complexes, we conducted DNA footprinting titrations for the high-affinity ([−]GC) and low-affinity sequence-specific sites ([+]TG). When cleaved by DNase I, a minor groove probe, both sites yielded footprints characteristic of sequence-specific ETS domain–DNA complexes. Specifically, the TTCC strand reveals a strong hypersensitive position at 5′-**T**p**T**p**C**p**C**pN$_\alpha$↓pN$_\beta$pT-3′ just 3′ to the core consensus (marked with an asterisk in Figure 5A), corresponding to the core consensus in the GGAA strand and caused by widening of the minor groove at the core consensus. As protein concentrations increase to $\geq 10^{-6}$ M, the magnitude of this hypersensitive band begins to diminish (Figure 5B). There are two possible reasons for the loss of DNase I hypersensitivity. Binding of the second equivalent of the PU.1 ETS domain may be blocking the minor groove at the core consensus in the 2:1 complex. Alternatively, the second equivalent may be blocking the minor groove 5′ or major groove 3′ to the hypersensitive position (on one side of the double helix), the access to both of which is also required by DNase I.[31] To distinguish between these possibilities, we probed the system under identical conditions with hydroxyl radicals ($^\bullet$OH), a hydration probe that attacks deoxyribose atoms in the minor groove (Figure 5C,D).[32] For both sites, $^\bullet$OH footprints were observed adjacent to the core consensus, consistent with protein contacts at the minor groove at those positions. The core consensus, which is solvent-exposed in the cocrystal structure in the 1:1 complex,[3] remains sensitive to $^\bullet$OH. At protein concentrations corresponding to the loss of hypersensitivity in the DNase I footprint, the $^\bullet$OH footprints show increased reactivity at the core consensus as well as additional protected positions immediately away from the core consensus (Figure 5E). Thus, accessibility to the minor groove at the core consensus is not the reason for reduced DNase I hypersensitivity. Rather, through direct occupancy or a change in conformation, the minor groove 5′ to the core consensus is occluded to DNase I in the 2:1 complex.

To assess additional sequence-specific changes in the protein–DNA interface induced by the 2:1 complex, we probed the major groove by permanganate (MnO_4^-) footprinting to take advantage of the abundant thymine residues in the TTCC strand (Figure 6). The two specific sites show clear differences in the reactivities of their T residues to $KMnO_4^-$ oxidation. Specifically, both T residues in the core consensus are substantially protected in the high-affinity [−]GC site but unprotected in the low-affinity [+]TG site. In the flanking segments, T residues exhibit variable protection and, in some cases, hypersensitivity that is clearly site-dependent. The most substantial differences (>0.3 in relative cleavage) are observed at the two core T residues (T_{+1} and T_{+2}) as well as flanking positions T_{-9}, T_{-7}, T_{-5}, T_{+7}, and T_{+8}. Finally, we note that positions immediately 3′ to the core consensus (N_{+3}–N_{+6} positions) are not strongly protected from $KMnO_4^-$, implying that the second equivalent of the PU.1 ETS domain is not binding in the 3′ major groove.

DISCUSSION

Various dimeric configurations involving ETS domains bound to DNA have been reported in the literature. These complexes involve either additional domains or binding partners for oligomerization [e.g., GABPα/β,[7] SRF in the case of SAP-1,[8] or the PNT domain in the case of TEL [33]] and/or composite binding sites harboring tandem consensus motifs.[34−36] These data demonstrate that the minimal ETS domain of PU.1 exists as a stable dimer not only in the free state but also when bound to a single specific DNA site. The dimer is not the preferred DNA-bound state but is induced in the presence of excess protein at relatively high concentrations ($\geq 10^{-6}$ M). Such concentrations were encountered in our ITC and footprinting experiments. Dimeric PU.1 ETS domains had not been detected in most reported investigations of this system because noncalorimetric techniques (e.g., filter binding, electrophoretic mobility shift, fluorescence anisotropy, surface plasmon resonance, and far-UV circular dichroism) typically employ lower protein concentrations.[2,15,19,29,30,37−39] In the DNA-free state, our DLS data show that dissociation and unfolding in the DNA-free state couple thermodynamically to give an apparently two-state denaturation. Thus, oligomeric effects would not be apparent in melting experiments performed at a single protein concentration.[29,30] Finally, the apparent negative cooperativity between DNA binding and protein dimerization is an important feature in interpreting these data with respect to known structural data for this system. As observed consistently in the ITC forward titrations (the Fα phase), at up to stoichiometric proportions of the ETS domain, even at high protein concentrations, the 1:1 complex is the exclusive DNA-bound state. Thus, the oligomeric properties of the ETS

dx.doi.org/10.1021/bi300331v | Biochemistry 2012, 51, 4096–4107

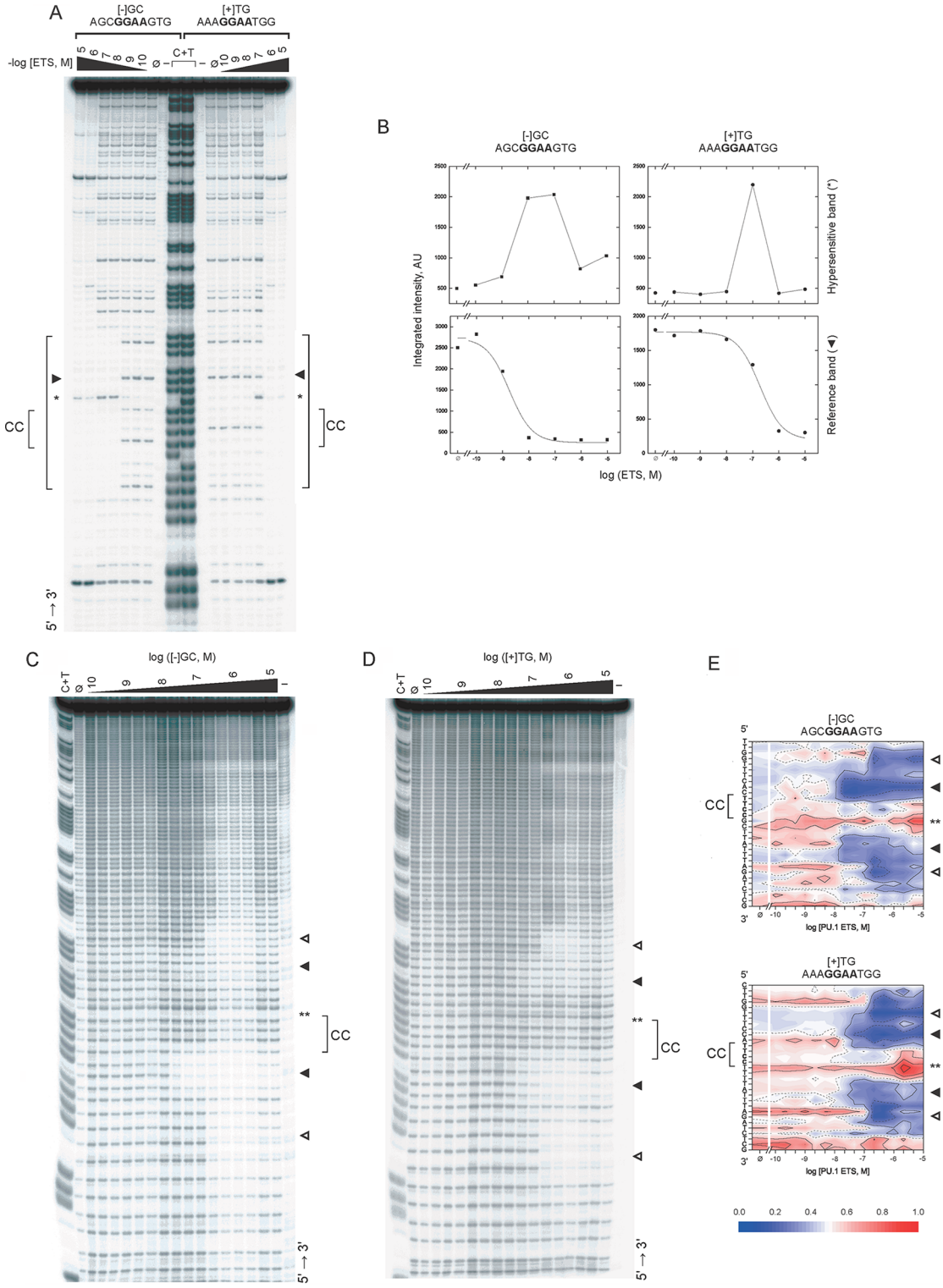

Figure 5. Quantitative DNA footprinting titrations resolve the topology of PU.1 ETS domain−DNA complexes. Radiolabeled DNA fragments harboring the high-affinity [−]GC or low-affinity [+]TG sequence-specific sites were titrated with the PU.1 ETS domain and probed by DNase I or hydroxyl radicals. (A) DNase I titrations of the TTCC strands of [−]GC and [+]TG sites. Uncut but ETS-saturated (−) and cut but ETS-free (ø) DNA were included as controls. Bands were identified by a C+T chemical sequencing reaction. Footprints of the 1:1 complex are marked with brackets. CC denotes the position of the core consensus. DNase I hypersensitive positions are marked with asterisks. (B) Titration profiles of the DNase I-hypersensitive positions (∗) for the [−]GC (■) and [+]TG (●) sites. Profiles for a nonhypersensitive, protected position (marked with arrowheads in panel A) are shown for comparison. (C and D) Hydroxyl radical footprints of the [−]GC and [+]TG sites. (E) Contour plot generated from the fitted integrated intensity at each of the indicated positions, normalized to intensities of an unprotected region outside the footprint. Contour lines represent 0.125 unit increments; selected contour lines were drawn solid only to highlight protected (blue) and hypersensitive (red) regions. Protected positions in the 1:1 complex are marked with black arrowheads, and additional protected positions in the 2:1 complex are marked with white arrowheads. Hypersensitive core positions are marked by double asterisks.

dx.doi.org/10.1021/bi300331v | *Biochemistry* 2012, 51, 4096−4107

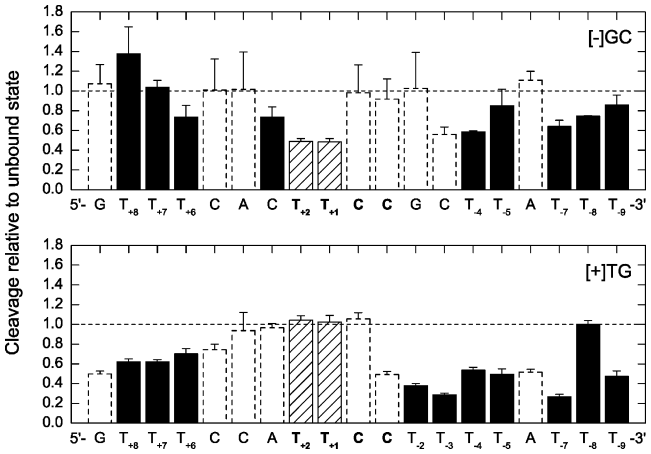

Figure 6. Probing the major groove of the 2:1 PU.1 ETS domain–DNA complex by quantitative permanganate (MnO_4^-) footprinting. Radiolabeled DNA fragments harboring the high-affinity [−]GC or low-affinity [+]TG sites alone or complexed with 10^{-5} M PU.1 ETS domain were probed with $KMnO_4$. The gel images and lane traces are provided as Figure S2 of the Supporting Information. For each position, the fitted integrated intensity corresponding to MnO_4^- reactivity in the complex was expressed as a ratio (±SE) relative to the unbound site. Subscripts denote the position of the base relative to the center of the core consensus. The two T residues in the core consensus (T_{+1} and T_{+2}) are shown as hatched bars. Flanking T residues are shown as solid bars. Non-T residues are shown as dashed outlines for reference.

domain reported here are not in conflict with the 1:1 stoichiometry observed in the cocrystal structure of the PU.1 ETS domain–DNA complex.[3] On the other hand, at concentrations comparable to those used in our ITC and LS experiments, NMR characterization of the unbound PU.1 ETS domain revealed perturbations in relaxation parameters consistent with self-association in solution.[40] These data are therefore consistent with, and substantially extend, known biophysical observations of the PU.1 ETS domain.

Nature of the PU.1 ETS Dimer. Limited details about ETS dimers exist. Our ITC data suggest that the DNA-bound PU.1 ETS dimer is a structurally asymmetric species. If it is a symmetric dimer in the DNA-bound state, apparent negative cooperativity observed in the reverse titrations (DNA into ETS) should be manifest in the forward titrations. However, the 2:1 protein:DNA stoichiometry observed in the forward titrations and a lack of heterogeneity in the titration heats in the Fα phase are incompatible with such a proposal. In the unbound state, analysis of NMR relaxation parameters as a function of protein sequence has identified 29 N-terminal residues that likely participate in self-association.[29,40] These residues are conformationally flexible and located opposite the DNA-binding surface. If dimerization is mediated by these residues in each subunit, the PU.1 ETS dimer is likely symmetric in the DNA-free state. We may therefore infer that the dimeric structures in the DNA-bound and free states are distinct.

Expansion of the site-specific $^{\bullet}$OH footprints suggests that part of the DNA binding surface of the second equivalent is diverted to new contacts not present in the 1:1 complex. This would account for the apparent failure of the second equivalent to bind another sequence-specific oligo in the forward ITC titrations. For both sequences, induced sensitivity to $^{\bullet}$OH at the core consensus is substantially increased in the 2:1 complex relative to that in the 1:1 complex. This observation is consistent with further distortion of the minor groove, a feature that is consistent with increased local curvature in the bound DNA.[41] Sequence dependence appears to operate as $^{\bullet}$OH cleavage is enhanced for the [+]TG site relative to the [−]GC site. Additional support for sequence dependence is afforded by differences in reactivity to MnO_4^- for the two sites. Both T residues in the core consensus of the high-affinity [−]GC site are >50% protected but unprotected in the low-affinity [+]TG site, a feature that mirrors a corresponding reactivity of the core G residues to DMS.[16] Reactivities among the flanking T residues are more variable but also sequence-dependent. The majority of these residues become less reactive in the 2:1 complex than in unbound DNA. Because they are also protected from $^{\bullet}$OH in the minor groove, it seems unlikely that a concurrent blockade of the major groove is occluding access for the oxidant. Oxidation of thymine's C5=C6 bond by MnO_4^- requires access from above or below the plane of the base.[42] Therefore, the reduced reactivity among flanking T residues likely indicates an increased level of stacking of the bases in the protein–DNA complex.[43]

Enhanced base stacking can be accomplished by overwinding the DNA (increased helical twist) with an attendant decrease in groove widths. In the 1:1 complex,[3] insertion of the recognition helix of the ETS domain at the core consensus leads to curvature into the major groove and expansion of the opposite minor groove (Figure S3 of the Supporting Information). For the 2:1 complex, our footprinting data support a model in which the core consensus is additionally curved into the major groove, leading to further expansion of the minor groove that is relieved by groove compression in the flanking segments (Figure 7). This model is compatible with the observed sequence-dependent differences in the footprints for the two sites. Thus, relative to the high-affinity [−]GC site, the low-affinity [+]TG site exhibits both stronger $^{\bullet}$OH cleavage in the core consensus (consistent with increased local curvature) and reduced reactivity with respect to MnO_4^- in the flanking sequences in all flanking T residues from T_{-7} to T_{+8} (consistent with an increased level of base stacking caused by local overwinding or groove compression). In light of the model, the strong protection of the flanking A_4 tract in the [−] segment of the [+]TG site (T_{-2} to T_{-5}) is particularly striking because A tracts are typically less susceptible to attack by MnO_4^- relative to random-sequence DNA in the first place.[43]

Thermodynamic analysis according to Scheme 1 indicates that PU.1 ETS dimerization is entropy-driven at 25 °C and 150 mM Na^+ in both the DNA-bound and -free states. This is consistent with dehydration of surfaces accompanying van der Waals or hydrophobic interactions by the N-terminal residues identified by NMR.[29,40] The entropic contributions to dimerization are even higher in the DNA-bound state (the Fβ phase) and may reflect additional contributions from new contacts with the DNA backbone in the 2:1 complex. Importantly, the thermodynamics for forming this complex are strongly dependent on the DNA site examined (Figure 4). Not only are the enthalpic and entropic contributions correlated with binding affinity, the associated changes in heat capacity vary significantly for the two sites. Moreover, the effect of salt is also sequence-dependent. Whereas $\Delta H_{F\beta}$ for the low-affinity [+]TG site is essentially insensitive to Na^+ from 150 to 250 mM, the high-affinity [−]GC site is highly sensitive in terms of both enthalpy and ΔC_p. These thermodynamic differences imply that the structure of the 2:1 ternary complex is sequence-dependent,

dx.doi.org/10.1021/bi300331v | *Biochemistry* 2012, 51, 4096–4107

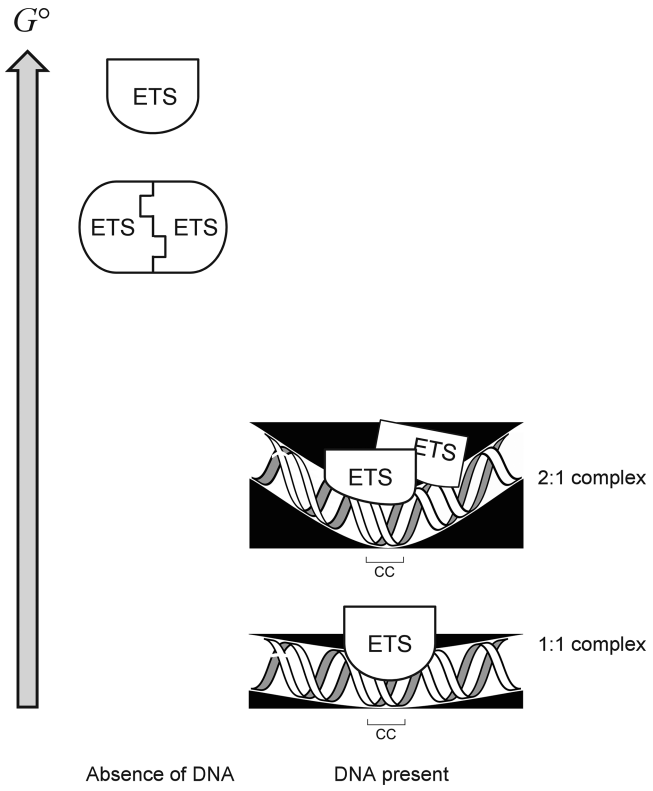

Figure 7. Schematic model of PU.1 ETS domain−DNA interactions in solution. Under standard state conditions, the PU.1 ETS monomer is unstable with respect to the dimer in the absence of DNA. The 1:1 DNA-bound complex is the most stable but is induced to a 2:1 complex in the presence of excess DNA. The magnitudes of $\Delta G°$ (represented by vertical distances) among the free ETS dimer and the DNA-bound states would depend on the binding site considered. The schematic shapes of the ETS domain are drawn only to help distinguish the various states. In the 1:1 complex,[3] the binding site is curved into the major groove at the core consensus (labeled CC), as observed in the cocrystal structure with a high-affinity site (Protein Data Bank entry 1PUE; Figure S3 of the Supporting Information). The minor groove at CC is locally expanded to accommodate this curvature. On the basis of our footprinting data, the 2:1 complex is further curved at CC. The additional required expansion of the minor groove at CC is relieved by local groove compression achieved by overwinding (increased helical twist) of the flanking segments.

and that sequence identity of a DNA site can dictate distal protein−protein interactions.

Biological Implications of Self-Association of the ETS Domain. Homodimerization by full-length ERG, Elk-1 Ets-1, PU.1, and the obligate involvement of their ETS domains have been documented.[12−14,44] Homodimerization by ETS proteins has been implicated in their cytoplasmic stability against proteosomal degradation, nuclear localization, and gene transactivation.[12,13] A general theme of ETS-mediated self-association as a negative regulator of nuclear targeting and transactivation is emerging. Because ETS domains share strong structural conservation despite limited sequence homology,[41] heterotypic dimers of different ETS proteins and their isoforms have also been observed.[14,44] While not all combinations of ETS proteins are apparently possible, the biophysical basis of this "selectivity" is as yet unclear.

Mutual exclusivity between self-association and binding to a single sequence-specific site is part of the current paradigm in ETS domain−DNA interactions. These data clearly demonstrate that two minimal ETS domains can "co-occupy" a single specific site. While the 2:1 complex is not preferred versus the 1:1 complex, it has reasonable affinity in solution ($K_D \sim 10^{-6}$ M) as judged by the DNase I and •OH footprints at this protein concentration. Because the crowded cellular milieu (10^2 g/L in solute) strongly promotes self-association and formation of the complex,[45,46] the potential biological relevance of this phenomenon merits further investigation.

Self-association of the PU.1 ETS domain is also relevant in terms of interactions with non-ETS binding partners. The tendency of the PU.1 ETS domain for self-association predicts interactions with binding partners.[40] Conformationally flexible residues that are implicated in self-association also participate in recruiting IRF-4 to a composite DNA binding site.[29] In addition to the ETS domain, contacts emanating from elsewhere in PU.1 (the PEST domain) are involved.[29,39,47] Nonetheless, as with several other examples,[14] the ETS domain is the keystone protein−protein interaction domain. These data clearly demonstrate an intrinsic ability to bind DNA to regulate self-association by an ETS domain and to do so in a sequence-dependent manner. In view of the emerging relevance of homodimerization and PU.1−binding partner interactions,[48] the data described herein suggest a previously unrecognized role for the intrinsic sequence selectivity by PU.1, and possibly other ETS transcription factors.

■ ASSOCIATED CONTENT

Supporting Information

Figures S1−S3. This material is available free of charge via the Internet at http://pubs.acs.org.

■ AUTHOR INFORMATION

Corresponding Author

*P.O. Box 646534, Pullman, WA 99164-6534. Telephone: (509) 335-8341. Fax: (509) 335-5902. E-mail: gpoon@wsu.edu.

Funding

This investigation was financially supported by the College of Pharmacy, Washington State University, and American Cancer Society Institutional Research Grant IRG-77-003-27 to G.M.K.P.

Notes

The authors declare no competing financial interest.

■ ACKNOWLEDGMENTS

We thank Ms. Crystal Van Dyken and Mr. Victor M. Bii for technical assistance.

■ ABBREVIATIONS

ITC, isothermal titration calorimetry; SEC, size-exclusion chromatography; LS, light scattering; SLS, static light scattering; DLS, dynamic light scattering; OH, hydroxyl radical; SE, standard error.

■ REFERENCES

(1) Wei, G. H., Badis, G., Berger, M. F., Kivioja, T., Palin, K., Enge, M., Bonke, M., Jolma, A., Varjosalo, M., Gehrke, A. R., Yan, J., Talukder, S., Turunen, M., Taipale, M., Stunnenberg, H. G., Ukkonen, E., Hughes, T. R., Bulyk, M. L., and Taipale, J. (2010) Genome-wide analysis of ETS-family DNA-binding *in vitro* and *in vivo*. *EMBO J. 29*, 2147−2160.

(2) Szymczyna, B. R., and Arrowsmith, C. H. (2000) DNA binding specificity studies of four ETS proteins support an indirect read-out mechanism of protein-DNA recognition. *J. Biol. Chem. 275*, 28363−28370.
(3) Kodandapani, R., Pio, F., Ni, C. Z., Piccialli, G., Klemsz, M., McKercher, S., Maki, R. A., and Ely, K. R. (1996) A new pattern for helix-turn-helix recognition revealed by the PU.1 ETS-domain-DNA complex. *Nature 380*, 456−460.
(4) Li, S. L., Schlegel, W., Valente, A. J., and Clark, R. A. (1999) Critical flanking sequences of PU.1 binding sites in myeloid-specific promoters. *J. Biol. Chem. 274*, 32453−32460.
(5) Escalante, C. R., Brass, A. L., Pongubala, J. M. R., Shatova, E., Shen, L., Singh, H., and Aggarwal, A. K. (2002) Crystal Structure of PU.1/IRF-4/DNA Ternary Complex. *Mol. Cell 10*, 1097−1105.
(6) Hollenhorst, P. C., McIntosh, L. P., and Graves, B. J. (2011) Genomic and biochemical insights into the specificity of ETS transcription factors. *Annu. Rev. Biochem. 80*, 437−471.
(7) Batchelor, A. H., Piper, D. E., de la Brousse, F. C., McKnight, S. L., and Wolberger, C. (1998) The structure of GABPα/β: An ETS domain-ankyrin repeat heterodimer bound to DNA. *Science 279*, 1037−1041.
(8) Hassler, M., and Richmond, T. J. (2001) The B-box dominates SAP-1-SRF interactions in the structure of the ternary complex. *EMBO J. 20*, 3018−3028.
(9) Garvie, C. W., Hagman, J., and Wolberger, C. (2001) Structural studies of Ets-1/Pax5 complex formation on DNA. *Mol. Cell 8*, 1267−1276.
(10) Kim, W. Y., Sieweke, M., Ogawa, E., Wee, H. J., Englmeier, U., Graf, T., and Ito, Y. (1999) Mutual activation of Ets-1 and AML1 DNA binding by direct interaction of their autoinhibitory domains. *EMBO J. 18*, 1609−1620.
(11) Goetz, T. L., Gu, T. L., Speck, N. A., and Graves, B. J. (2000) Auto-inhibition of Ets-1 is counteracted by DNA binding cooperativity with core-binding factor α2. *Mol. Cell. Biol. 20*, 81−90.
(12) Drewett, V., Muller, S., Goodall, J., and Shaw, P. E. (2000) Dimer formation by ternary complex factor ELK-1. *J. Biol. Chem. 275*, 1757−1762.
(13) Evans, E. L., Saxton, J., Shelton, S. J., Begitt, A., Holliday, N. D., Hipskind, R. A., and Shaw, P. E. (2011) Dimer formation and conformational flexibility ensure cytoplasmic stability and nuclear accumulation of Elk-1. *Nucleic Acids Res. 39*, 6390−6402.
(14) Carrère, S., Verger, A., Flourens, A., Stehelin, D., and Duterque-Coquillaud, M. (1998) Erg proteins, transcription factors of the Ets family, form homo, heterodimers and ternary complexes via two distinct domains. *Oncogene 16*, 3261−3268.
(15) Poon, G. M., and Macgregor, R. B., Jr. (2003) Base coupling in sequence-specific site recognition by the ETS domain of murine PU.1. *J. Mol. Biol. 328*, 805−819.
(16) Poon, G. M. K. (2012) Sequence discrimination by the DNA-binding domain of the ETS-family transcription factor PU.1 is linked to specific hydration of the protein-DNA interface. *J. Biol. Chem.*, DOI: 10.1074/jbc.M112.342345.
(17) Tataurov, A. V., You, Y., and Owczarzy, R. (2008) Predicting ultraviolet spectrum of single stranded and double stranded deoxyribonucleic acids. *Biophys. Chem. 133*, 66−70.
(18) Poon, G. M. (2010) Explicit formulation of titration models for isothermal titration calorimetry. *Anal. Biochem. 400*, 229−236.
(19) Poon, G. M., and Macgregor, R. B., Jr. (2004) A thermodynamic basis of DNA sequence selectivity by the ETS domain of murine PU.1. *J. Mol. Biol. 335*, 113−127.
(20) Ha, J. H., Spolar, R. S., and Record, M. T., Jr. (1989) Role of the hydrophobic effect in stability of site-specific protein-DNA complexes. *J. Mol. Biol. 209*, 801−816.
(21) Leblanc, B., and Moss, T. (2001) DNase I footprinting. *Methods Mol. Biol. 148*, 31−38.
(22) Tullius, T. D., and Dombroski, B. A. (1986) Hydroxyl radical "footprinting": High-resolution information about DNA-protein contacts and application to lambda repressor and Cro protein. *Proc. Natl. Acad. Sci. U.S.A. 83*, 5469−5473.
(23) Sekiguchi, J., and Shuman, S. (1996) Covalent DNA binding by vaccinia topoisomerase results in unpairing of the thymine base 5′ of the scissile bond. *J. Biol. Chem. 271*, 19436−19442.
(24) Shadle, S. E., Allen, D. F., Guo, H., Pogozelski, W. K., Bashkin, J. S., and Tullius, T. D. (1997) Quantitative analysis of electrophoresis data: Novel curve fitting methodology and its application to the determination of a protein-DNA binding constant. *Nucleic Acids Res. 25*, 850−860.
(25) Eisenbeis, C. F., Singh, H., and Storb, U. (1993) PU.1 is a component of a multiprotein complex which binds an essential site in the murine immunoglobulin lambda 2-4 enhancer. *Mol. Cell. Biol. 13*, 6452−6461.
(26) Kuehner, D. E., Heyer, C., Rämsch, C., Fornefeld, U. M., Blanch, H. W., and Prausnitz, J. M. (1997) Interactions of lysozyme in concentrated electrolyte solutions from dynamic light-scattering measurements. *Biophys. J. 73*, 3211−3224.
(27) Wilson, L. J., Adcock-Downey, L., and Pusey, M. L. (1996) Monomer concentrations and dimerization constants in crystallizing lysozyme solutions by dialysis kinetics. *Biophys. J. 71*, 2123−2129.
(28) Hellberg, U., Ivarsson, J.-P., and Johansson, B.-L. (1996) Characteristics of Superdex prep grade media for gel filtration chromatography of proteins and peptides. *Process Biochem. (Oxford, U.K.) 31*, 163−172.
(29) McKercher, S. R., Lombardo, C. R., Bobkov, A., Jia, X., and Assa-Munt, N. (2003) Identification of a PU.1-IRF4 protein interaction surface predicted by chemical exchange line broadening. *Proc. Natl. Acad. Sci. U.S.A. 100*, 511−516.
(30) Poon, G. M., Gross, P., and Macgregor, R. B., Jr. (2002) The sequence-specific association of the ETS domain of murine PU.1 with DNA exhibits unusual energetics. *Biochemistry 41*, 2361−2371.
(31) Suck, D., and Oefner, C. (1986) Structure of DNase I at 2.0 Å resolution suggests a mechanism for binding to and cutting DNA. *Nature 321*, 620−625.
(32) Balasubramanian, B., Pogozelski, W. K., and Tullius, T. D. (1998) DNA strand breaking by the hydroxyl radical is governed by the accessible surface areas of the hydrogen atoms of the DNA backbone. *Proc. Natl. Acad. Sci. U.S.A. 95*, 9738−9743.
(33) Green, S. M., Coyne, H. J., III, McIntosh, L. P., and Graves, B. J. (2010) DNA binding by the ETS protein TEL (ETV6) is regulated by autoinhibition and self-association. *J. Biol. Chem. 285*, 18496−18504.
(34) Babayeva, N. D., Wilder, P. J., Shiina, M., Mino, K., Desler, M., Ogata, K., Rizzino, A., and Tahirov, T. H. (2010) Structural basis of Ets1 cooperative binding to palindromic sequences on stromelysin-1 promoter DNA. *Cell Cycle 9*, 3054−3062.
(35) Agarkar, V. B., Babayeva, N. D., Wilder, P. J., Rizzino, A., and Tahirov, T. H. (2010) Crystal structure of mouse Elf3 C-terminal DNA-binding domain in complex with type II TGF-β receptor promoter DNA. *J. Mol. Biol. 397*, 278−289.
(36) Kopp, J. L., Wilder, P. J., Desler, M., Kinarsky, L., and Rizzino, A. (2007) Different domains of the transcription factor ELF3 are required in a promoter-specific manner and multiple domains control its binding to DNA. *J. Biol. Chem. 282*, 3027−3041.
(37) Gross, P., Yee, A. A., Arrowsmith, C. H., and Macgregor, R. B., Jr. (1998) Quantitative hydroxyl radical footprinting reveals cooperative interactions between DNA-binding subdomains of PU.1 and IRF4. *Biochemistry 37*, 9802−9811.
(38) Pió, F., Assa-Munt, N., Yguerabide, J., and Maki, R. A. (1999) Mutants of ETS domain PU.1 and GGAA/T recognition: Free energies and kinetics. *Protein Sci. 8*, 2098−2109.
(39) Yee, A. A., Yin, P., Siderovski, D. P., Mak, T. W., Litchfield, D. W., and Arrowsmith, C. H. (1998) Cooperative interaction between the DNA-binding domains of PU.1 and IRF4. *J. Mol. Biol. 279*, 1075−1083.
(40) Jia, X., Lee, L. K., Light, J., Palmer, A. G., III, and Assa-Munt, N. (1999) Backbone dynamics of a short PU.1 ETS domain. *J. Mol. Biol. 292*, 1083−1093.
(41) Pió, F., Kodandapani, R., Ni, C. Z., Shepard, W., Klemsz, M., McKercher, S. R., Maki, R. A., and Ely, K. R. (1996) New insights on

DNA recognition by ETS proteins from the crystal structure of the PU.1 ETS domain-DNA complex. *J. Biol. Chem. 271*, 23329−23337.
(42) Hayatsu, H., and Ukita, T. (1967) The selective degradation of pyrimidines in nucleic acids by permanganate oxidation. *Biochem. Biophys. Res. Commun. 29*, 556−561.
(43) McCarthy, J. G., Williams, L. D., and Rich, A. (1990) Chemical reactivity of potassium permanganate and diethyl pyrocarbonate with B DNA: Specific reactivity with short A-tracts. *Biochemistry 29*, 6071−6081.
(44) Jousset, C., Carron, C., Boureux, A., Quang, C. T., Oury, C., Dusanter-Fourt, I., Charon, M., Levin, J., Bernard, O., and Ghysdael, J. (1997) A domain of TEL conserved in a subset of ETS proteins defines a specific oligomerization interface essential to the mitogenic properties of the TEL-PDGFR β oncoprotein. *EMBO J. 16*, 69−82.
(45) Hall, D., and Minton, A. P. (2003) Macromolecular crowding: Qualitative and semiquantitative successes, quantitative challenges. *Biochim. Biophys. Acta 1649*, 127−139.
(46) Alice, B. F. (1982) How crowded is the cytoplasm? *Cell 30*, 345−347.
(47) Perkel, J. M., and Atchison, M. L. (1998) A Two-Step Mechanism for Recruitment of Pip by PU.1. *J. Immunol. 160*, 241−252.
(48) Gupta, P., Gurudutta, G. U., Saluja, D., and Tripathi, R. P. (2009) PU.1 and partners: Regulation of haematopoietic stem cell fate in normal and malignant haematopoiesis. *J. Cell. Mol. Med. 13*, 4349−4363.